Numerical assessment of ICRF-specific plasma-wall interaction in the new ITER baseline using the SSWICH-SW code

Nuclear Materials and Energy 42 (2025) 101831

Contents lists available at ScienceDirect

Nuclear Materials and Energy

journal homepage: www.elsevier.com/locate/nme

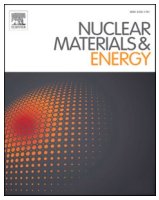

Numerical assessment of ICRF-specific plasma-wall interaction in the new ITER baseline using the SSWICH-SW code

L. Colas [a,*], W. Helou [b], G. Urbanczyk [c,d], V. Bobkov [d], F. Calarco [b], N. Fedorczak [a], D. Milanesio [e], J. Hillairet [a]

[a] CEA, IRFM, F-13108 Saint-Paul-Lez-Durance, France
[b] ITER Organization, Route de Vinon-sur-Verdon, CS 90 046, 13067 St. Paul Lez Durance Cedex, France
[c] Institut Jean Lamour, UMR 7198 CNRS-Université de Lorraine, Campus Artem, 2 allée André Guinier, 54011 Nancy, France
[d] Max-Planck-Institut für Plasmaphysik, Boltzmannstr. 2, 85748 Garching, Deutschland, Germany
[e] Departement of Electronics, Politecnico di Torino, Italy

ARTICLE INFO

Keywords:
ICRF
RF sheath
ITER
W sputtering
Local gas puffing
Numerical simulation

ABSTRACT

In 2023, switching the material on the first wall of ITER to tungsten (W) was recommended. In magnetic Fusion devices, waves in the Ion Cyclotron Range of Frequencies (ICRF) interact with the Scrape-Off Layer (SOL) *via* RF-sheath rectification. This contribution re-assesses this phenomenon close to the ITER ICRF antenna, focusing on the ICRF-specific gross erosion of W from the antenna port sides. Our quantitative estimates rely on predictive multi-2D numerical simulations of the ICRF antenna environment using the SSWICH-SW code. They combine Slow Wave propagation from the antenna mouth to the SOL, the excitation of RF oscillations in the sheath voltages at the antenna port sides and a subsequent DC biasing of the SOL. Maps of the parallel RF electric field at the antenna mouth, from the antenna code TOPICA, excite the system. Our simulations cover more than four decades in the local densities near the antenna. Since both the sputtering and the local heat loads are proportional to the local particle fluxes, the most intense Plasma-Wall Interaction is found for high local density, with or without ICRF waves. In these conditions, larger margins also exist for coupling the ICRF power. We tested several operational trade-offs between these two constraints. The simulated target plasma contains 2% of neon ions. These are efficient at sputtering W, already at low accelerating voltages. Consequently, although the RF-sheath rectification sufficiently amplifies the local sputtering at the antenna port for a detection using visible spectroscopy, the ICRF-induced increment of the gross W production represents at worse 22% of the W source expected from thermal sheaths over the eighteen out-board mid-plane ports. An upper bound, independent of our main assumptions, is proposed for this enhancement factor. This moderate expected global increase questions the ability to detect ICRF-specific W contamination of the plasma core, even at the planned maximal ICRF power.

1. Introduction

In 2023, a major rebaseline was proposed in ITER [1]. It recommended switching the material on its first wall to tungsten (W). The outer wall could then represent a large area of high-*Z* material subject to erosion from the plasma. In present magnetic Fusion devices, the high-*Z* impurities originating from the outer mid-plane of the main chamber are generally badly screened, see *e.g.* [2]. With the planned new configuration, a risk therefore exists of excessive contamination of the core plasma with W. The revised baseline plans that one outer mid-plane port of ITER will host a phased strap array in the Ion Cyclotron Range of Frequencies (ICRF) [3]. In the first phase of operation, the Start of Research Operation (SRO), this ICRF system will be tested on plasma at a 10 MW power level, in view of a possible upgrade to 20 MW. In magnetic Fusion devices, ICRF waves interact with the Scrape-Off Layer (SOL) *via* Radio-Frequency (RF)-sheath rectification, resulting in locally enhanced Plasma-Wall Interaction (PWI) [4]. An earlier ITER study focussed on ICRF-specific heat loads, the main risk in the previous beryllium environment [5,6]. Using an upgraded simulation tool, this contribution emphasizes the ICRF-specific gross erosion of W from the antenna port sides. Reference [7] reports a similar assessment using near-field based extrapolations from ASDEX Upgrade experimental results. The paper

* Corresponding author.
E-mail address: laurent.colas@cea.fr (L. Colas).

https://doi.org/10.1016/j.nme.2024.101831
Received 23 May 2024; Received in revised form 18 November 2024; Accepted 27 November 2024
Available online 30 November 2024

addresses:

1) Which conditions exacerbate the ICRF-specific PWI?
2) Do techniques exist to mitigate it? How do they affect the other functions of the ICRF antenna, primarily its ability to launch ICRF waves in the Fast Mode towards the plasma core?
3) How intense is the ICRF-specific contribution compared to other ICRF-independent PWI? As a reference, we estimate the contribution of thermal sheaths on the outer mid-plane ports, using the same simulation tools and input parameters as for RF-sheath rectification.
4) What can be tested experimentally during the SRO and how?

Reference [8], available on request, presents a more comprehensive report.

2. Simulation procedure

2.1. Coupled RF wave propagation and DC plasma biasing

Sheath rectification estimates rely on numerical simulations of the ICRF antenna environment with the SSWICH-SW code [9,10]. Using the multi-physics finite element solver COMSOL, SSWICH-SW combines RF Wave propagation from the antenna mouth to the SOL, the excitation of RF oscillations V_{RF} in the sheath voltages at the antenna port sides and a subsequent Direct Current (DC) biasing of the SOL.

Magnetized plasmas are bi-refringent dielectric materials: for given wave frequency and wave-vector parallel to $\mathbf{B_0}$, two types of plane waves, called Fast and Slow Waves, are allowed to propagate, with specific polarization and normal wavevector. ICRF antennas are meant to launch Fast Waves but also excite the Slow mode parasitically. The parallel RF electric field at the antenna mouth is attributed to the Slow wave. In a geometry where the walls are either parallel or normal to $\mathbf{B_0}$, only Slow waves are supposed to excite RF sheaths [11], which motivates focussing on this mode only. Recent 3D full-wave codes equivalent to SSWICH [12–14] remove this limitation but were not so far applied extensively to large antennas. Reference [12] checked, on a simpler case, that the Slow mode is indeed the main contributor to RF sheath excitation on walls that are acessible to this wave mode (*i.e.* close to the active antennas). Fig. 1 sketches the 2-dimensional (2D: radial/parallel) simulation domain. It includes a private SOL in grey representing the antenna port, followed by a free SOL where the Slow Mode can propagate. RF sheaths are treated as RF and DC boundary conditions applied at both sides of the antenna port (blue boundaries) where we assess the PWI. The output of an external 3D antenna code is needed as an input for our 2D SSWICH simulations. The 3D version of SSWICH (ref. [12]) removes this limitation. To excite the Slow mode, we impose at the antenna mouth (magenta boundary) maps of the near parallel RF electric field $E_{//}$ from the 3D antenna code TOPICA [15]. TOPICA was run with vacuum close to the antenna and a plasma a few centimetres in front of it. Reference [16] checked that the coupling results do not depend sensitively on the thickness of this vacuum layer, as long as the R-cutoff layer for the fast wave remains at the correct radial position.

Because it is non-linear, the time-averaged I_{DC}/V_{DC} electrical characteristic of a sheath gets distorted in the presence of an oscillating sheath potential V_{RF}. In practice, an electrically grounded wall element subject to sheath oscillations behaves as an electrode biased to DC potential $V_b(|V_{RF}|)$ with respect to the ground. The reaction of the plasma is generally a shift of its electric potential V_{DC} with respect to the grounded walls, in analogy with biased Langmuir probes. This self-biasing process is reviewed theoretically in reference [11] and experimentally in [4]. The DC biasing module of SSWICH-SW solves for the continuity of DC currents circulating in the SOL [4], in the presence of strongly anisotropic DC plasma conductivity due to the confinement magnetic field [17], DC sheaths at the walls and RF-induced wall self-bias V_b applied on the blue boundaries. Reference [10] addressed the role of the DC plasma conductivity on the PWI. In the ITER case, the detailed report [8] includes a scan of the DC plasma conductivity and illustrates its consequences on the PWI.

As SSWICH-SW simulates only the Slow Mode, it allows boundaries either parallel or normal to $\mathbf{B_0}$. The geometry of the ITER antenna port therefore needed idealization. In Fig. 1, it represents a rectangular zone with walls normal to $\mathbf{B_0}$. From the 3D CAD models of the ITER antenna in [18], the radial recess of the ICRF antenna in its port was adjusted to $L_\perp = 7$ mm all over the antenna height. As the actual first wall of ITER is shaped [3], choosing the parallel extent $L_{//}$ of the rectangle was more delicate. As a conservative assumption for PWI estimates [6,8], we placed the port sides as close toroidally as possible to the antenna mouth: $L_{//} = 1.67$ m, all over the radial depth of the antenna port. Reference [8] scanned $L_{//}$ and $L_\perp$

One multi-2D simulation gathers 271 independent 2D runs of SSWICH-SW depicted in Fig. 1, one every centimetre vertically along the antenna mouth. SSWICH-SW was tested against experiments with the Tore Supra [10,6], ASDEX Upgrade [19,20] and JET ITER-like antennas [21]. In view of the ITER simulations, these experimental tests only partially validate the code:

– Sheath rectification was assessed mainly on the lateral sides of the ICRF antennas, and not at other locations. Simulating far-field RF-sheaths, although desirable, is presently considered as immature. In present devices, near-field RF-sheaths likely dominate the RF-specific W erosion, at least in situations with good single-pass absorption for the Fast Wave [4].

– The present ICRF antennas are equipped with private side limiters that can be easily assimilated to walls normal to $\mathbf{B_0}$. The ITER antenna is surrounded by shaped walls at shallow incidence with respect to $\mathbf{B_0}$. More recent codes offer more geometrical fidelity [12–14].

– The present modelling mainly explored a limited domain of "high densities" at the antenna limiters. Our simulations also include "low density" scenarios where the cold Slow Mode propagates along resonant cones emerging from the antenna mouth [22], up to a Lower Hybrid (LH) resonant layer where they are absorbed [23]. The transverse wavelength for cold collision-less Slow Waves gets null as they reach the LH resonance. Finite Element Modelling of their propagation therefore imposes a very fine meshing of the simulation domain and becomes untractable numerically at the resonance. To emulate the presence of the LH resonance, we damp artificially the emitted waves before the resonance using Perfectly Matched Layers (PMLs) [22] at the inner and lateral parts of the simulation domain (see Fig. 1). When the LH resonant layer intersects the material boundaries, it can also affect the RF sheath excitation locally. Unfortunately no present modelling tool is able to simulate this process in a reliable and experimentally validated way, so

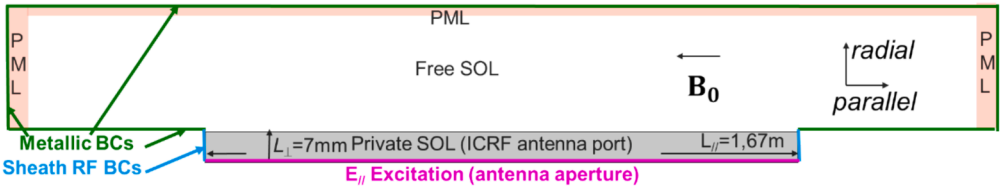

Fig. 1. 2D (radial/parallel) geometry of one SSWICH-SW run (not to scale). The reference dimensions of the idealized antenna port are indicated, as well as the boundary conditions (BCs) enforced at the different boundaries.

that we did not attempt this exercise.

2.2. Post-processing to assess parallel heat fluxes and wall sputtering at port sides

At each altitude y, SSWICH-SW produces profiles of the DC plasma potential $V_{DC}(x,y)$ along the two sides of the ICRF antenna port, as a function of the radial distance to the antenna mouth $x \equiv R_{ant}-R$. As an input, it receives profiles of density $n_e(x)$ and electron temperatures $T_e(x)$ [18]. Constant ratio T_i/T_e is assumed. The same radial distribution of density was used whatever the altitude y, which amounts to flattening the 3D geometry and the magnetic equilibrium poloidally. As the poloidal radius of curvature of the real antenna is larger than that of the magnetic surfaces, this flattening is a conservative assumption in terms of local particle fluxes onto the port sides. We assume that applying ICRF does not modify this background plasma, although present experiments frequently observe local $\mathbf{E} \times \mathbf{B_0}$ density convection in the strong gradients of V_{DC} [4,24,25]. Lower particle fluxes were observed at the center of convective cells, where sheath potentials are maximal [25]. The density modifications may therefore lower the overall PWI, although they could enhance it locally.

To assess the impurity contamination, one should ideally estimate the net W erosion from the wall. However uncertainty presently remains on the prompt redeposition factors in the case of RF sheaths, whose structure is quite different from usual thermal sheaths. We therefore sticked to the gross erosion. A key parameter for this purpose is the effective sputtering yield Y_{eff}, *i.e.* the probability for an ion impinging the wall to sputter a W atom. This probability depends on the energy of the ion when it hits the material boundaries. In our simulations, the walls are electrically grounded while the bulk plasma is (on average over time) at electric potential V_{DC}. Consequently an ion ionized Z times gains across the sheath the energy eZV_{DC}. In a multi-species plasma, Y_{eff} is a weighted average over the ion species. We assessed the PWI for a prescribed plasma composition in fuel and impurities [18]. This non-self-consistent mix is a conservative assumption in terms of absolute erosion levels. It was used all over our simulations, although more realistic mixtures may vary together with the SOL profiles [26]. Using a simple model, reference [7] also investigated a possible role of W self-sputtering. From tabulated sputtering data for each species in reference [27], one computes Y_{eff} for this mixture *versus* V_{DC}. The curve $Y_{eff}(V_{DC})$ was produced in the absence of sheath RF oscillations, although V_{RF} may also affect the ion energy distribution at the wall, when the RF period exceeds the ion transit time through the sheath [28–30]. For each simulation, we assessed the PWI with and without the ICRF power. In this latter case, the floating potential V_f without RF was used as the plasma DC potential V_{DC}.

Given our simplified geometry, we expressed the local PWI as parallel flux densities of impurities and heat. For overall estimates, these flux densities were subsequently integrated over the geometrical surface of the simulated port that shares the same area normal to $\mathbf{B_0}$ as the real ITER port: 7 mm radially × 2.7 m poloidally × 2 sides ~ 378 cm^2. Therefore the cumulated fluxes onto the antenna port sides are realistic. As these fluxes are proportional to the local parallel ion flux density onto the port side Γ_i, we will average below these quantities over the port surfaces using Γ_i as a weight function and denote these weighted averages $<\ldots>$. With this convention, the gross W source S_W over the port side writes

$$S_W \equiv \iint_{port\ side} \Gamma_W dxdy = \iint_{port\ side} Y_{eff}\Gamma_i dxdy = \langle Y_{eff}\rangle \iint_{port\ side} \Gamma_i dxdy \quad (1)$$

and similarly for ion power losses $P_{loss,i} = e\langle V_{DC} + 2.5T_i\rangle \iint_{port\ side}\Gamma_i dS$ and electron power losses $P_{loss,e} = 2e\langle kT_e \exp\left[e\left(V_b + V_f - V_{DC}\right)/kT_e\right]\rangle \iint_{port\ side}\Gamma_i dS$.

3. Main simulation results

3.1. Absolute PWI levels: The role of particle fluxes

A large uncertainty presently persists on the cross-field transport coefficients in the SOL. For given plasma parameters at the separatrix, this yields uncertain local plasma conditions near the ITER ICRF antenna [1]. Therefore we produced a database of 30 multi-2D simulations with a large variety of density profiles, representative of burning plasmas in the DT phase of ITER. Fig. 2 plots these profiles (from [18]) *versus* the radial distance x to the antenna. Dashed red curves represent rigid radial shifts of the "low 2010" magnetic configuration towards the antenna, by 2 and 5 cm. "Gas puff" refers to local gas injections on magnetic field lines connecting to the ICRF port (see [31,32] and section 3.4).

The grey region in Fig. 2 is the radial domain where we assess the PWI. Over all the scenarios, the density at the port entrance spans more than 4 orders of magnitude. The density decay length there is generally smaller than $L_\perp$, so that the effective wetted area is smaller than the surface of the port. The green horizontal domain sketches the density range for which the Slow Mode is propagative for the nominal local magnetic field near the antennas ($B_0 = 3.92$ T) and wave frequency 55 MHz, for a 50–50 % D-T plasma envisaged in the simulations. The upper bound of this domain is the Lower Hybrid (LH) resonance for the Slow Wave. For the studied scenarios, the SOL density in the antenna port region was either above or below this resonant density. We adapted the radial extent of the simulated free SOL to exclude the LH resonance from our simulation domain. Over our database, the largest values of $<V_{DC}>$ were found when the LH resonance was close to the antenna port, either behind or in front of it, so that its role on the PWI needs to be investigated further.

Equation (1) motivates plotting on Fig. 3 the expected gross W production S_W and the total expected power loss integrated over the ICRF port sides, *versus* Γ_i integrated over one port. As $\Gamma_i \propto n_e(T_e + T_i)^{1/2}$, the particle fluxes vary by more than 4 decades, primarily due to n_e (T_e ranges between 7 and 20 eV). In this diagram, the simulation points, with and without ICRF, occupy a band bounded by two tilted lines proportional to the total particle flux. Inside this band, a good correlation is found with the density profiles in Fig. 2. The horizontal spread of simulation points in the "low2010" scenario is mainly due to the radially shifted magnetic equilibria in Fig. 2. The cases slightly below and above the LH resonance near the antenna behave similarly.

From equation (1) the vertical distance between the two hatched lines, as well as the vertical shift between open and filled symbols, represent the relative variations in $<Y_{eff}>$ (factor of ~ 7 for gross sputtering) and mainly $<V_{DC}>$ (factor ~ 20 for heat loads) over our database. These relative variations, although significant, remain modest in comparison with those of Γ_i: the high-density scenarios exhibit the

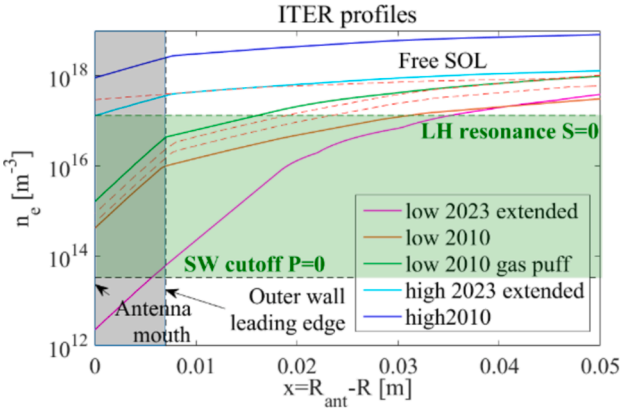

Fig. 2. Density profiles used for the present study *versus* radial distance to antenna mouth, together with characteristic densities for the slow mode.

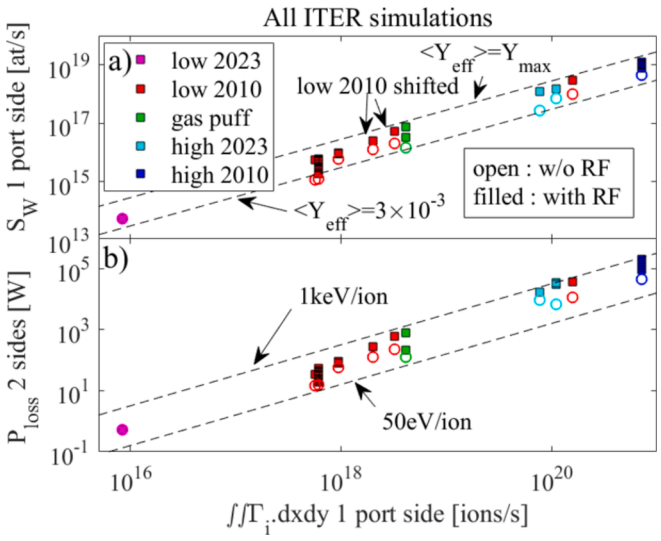

Fig. 3. A) total gross W source from and b) total power loss onto the ICRF port sides, *versus* total particle flux onto 1 port side. Same color codes for plasma profiles as on Fig. 2.

most intense gross W erosion [1]. This might be different for the core plasma contamination, due to possibly better impurity screening in the high-density SOL. For a fixed RF feeding scheme of the ITER strap array, Fig. 2 shows that the density at the ICRF antenna port generally correlates with the radial distance from the radiating straps to the typical R-cutoff layer for the Fast Wave. The scenarios with more intense PWI are therefore those for which larger margins exist for coupling the maximum RF power to the plasma, without exceeding a 45 kV peak voltage inside the antenna (the maximum voltage for coupling studies [3,15]). This stresses the need to find operational trade-offs between these two constraints.

3.2. Relative PWI during RF vs w/o RF

For given Γ_i, the gross W sputtering depends on the curve $Y_{eff}(V_{DC})$ in Fig. 4. Our plasma consists mainly of a 50–50 % D-T mix. The light impurity is neon, seeded to ease divertor detachment, with a relative abundance [Ne] = 2 %, split between the ionization stages 7^+ to 10^+. Traces of W^{2+} ions (relative abundance 10^{-4}) are also considered. The yellow region in Fig. 4 is the range of $<V_{DC}>$ spanned over our simulation database. In this region, neon ions dominate in the gross W erosion [1], whose magnitude is therefore proportional to [Ne]. Neon is efficient at sputtering, leading to large values of Y_{eff}, already at low V_{DC}: between the two boundaries of the yellow region, Y_{eff} "only" increases by a factor of 9. For accelerating voltages around 3 kV, Y_{eff} reaches an absolute maximum $Y_{max} \sim 2.8 \times 10^{-2}$.

Our exercise assumes that applying ICRF does not change Γ_i near the antenna. In the absence of RF-induced DC bias $V_b(|V_{RF}|)$, the expected DC plasma potential is the floating potential V_f. From equation (1), the RF-specific enhancement factor for the gross W sputtering in the ICRF port is $<Y_{eff}(V_{DC})>_{RF}/<Y_{eff}(eV_f)>$, independent of absolute Γ_i values. Fig. 5.a plots this numerical factor *versus* V_f. Consistent with Fig. 4, it is within a factor of 5 over our simulation database. Fig. 4 indicates an absolute upper bound for this enhancement factor: $Y_{max}/Y_{eff}(V_f) < 11$. It is overlaid in Fig. 5.a.

While the « local » enhancement factor for S_W at the ICRF port is relevant to estimate the lifetime of the port panels, it is also worth estimating an enhancement factor over the 18 outboard ports of ITER. This more "global" indicator is useful to estimate an evolution in the core contamination with W. To this end, we assume that all the ITER ports are similar in shape and experience similar density and temperature distributions as the ICRF port. Also implicit is that the impurities penetrate similarly from all the ports. These assumptions appear reasonable, except when gas is puffed locally (see section 3.4). The ICRF antenna occupies $N_{IC} = 1$ of these $N_{port} = 18$ ports. In present machines the PWI is amplified not everywhere but mainly on active ICRF antennas [33], although "remote W sources" may also exist [4,7]. Consequently we postulate that only the ICRF port experiences sheath rectification, while the other ports undergo thermal sheaths. The global enhancement factor F is then

$$F = 1 + \frac{N_{IC}}{N_{port}}\left[\frac{\langle Y_{eff}(V_{DC})\rangle_{RF}}{Y_{eff}(eV_f)} - 1\right] < 1 + \frac{N_{IC}}{N_{port}}\left[\frac{Y_{max}}{Y_{eff}(eV_f)} - 1\right] \equiv F_{max} \quad (2)$$

As long as neon ions dominate Y_{eff} in our mix, F weakly depends on [Ne]. With $T_e = 20$ eV and $T_i = 40$ eV, F-1 cannot exceed F_{max}-1=+20 %. This moderate increment reflects the modest fraction of outer wall area affected by sheath rectification, and the efficient sputtering of tungsten by thermal sheaths [1]. This latter argument also explains that the upper bounds decrease with increasing V_f in Fig. 5. F_{max} is independent of the RF-sheath code, of the port geometry and of the density profile, the main assumptions in our estimates. Since Y_{max} appears outside the yellow

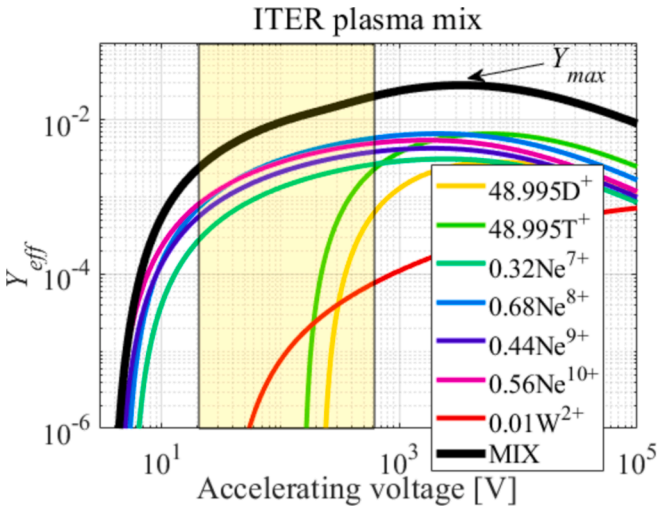

Fig. 4. Effective sputtering yield *versus* accelerating voltage V_{DC}, for the plasma composition envisaged in our simulations. The figure also dispatches Y_{eff} between the species in the plasma.

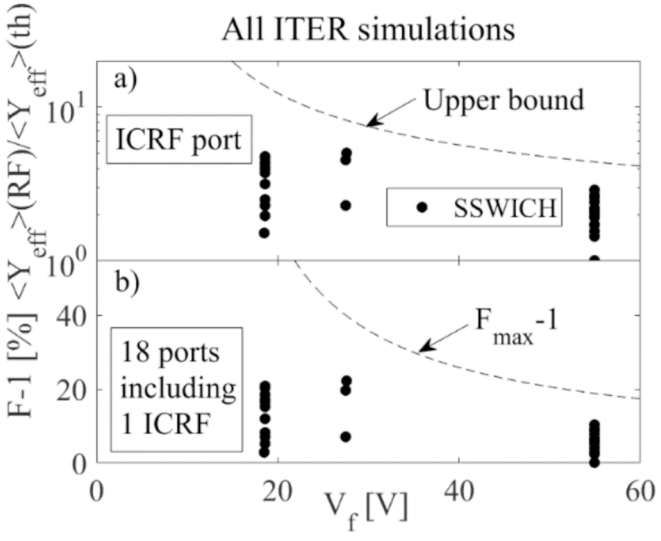

Fig. 5. Enhancement factors for gross W production a) over ICRF port sides and b) over 18 ITER ports, *versus* floating potential.

region in Fig. 4, our simulation points never reach these limits that can be considered as conservative. In practice, over our simulations, Fig. 5.b shows that F-1 does not exceed + 22 %, except with local gas puffing (see section 3.4).

3.3. PWI over ICRF power scan, observability of ICRF effects

To illustrate the previous sections concretely, Fig. 6 shows how S_W evolves over a scan of the ICRF power P_{RF}. We primarily performed erosion estimates with the "High 2010" density profile, already used in [6] as the most critical in terms of absolute PWI (see Fig. 3). The antenna feeding scheme was [0π0π] phasing with balanced power between the four toroidal columuns of straps. This configuration allows the ITER antenna to couple more than 20 MW [15]. We scanned P_{RF} up to 20 MW by rescaling the input $E_{//}$ field map as $P_{RF}{}^{1/2}$. At this maximum power level, S_W from the ICRF port increases by a factor ~ 2.7 compared to its value without ICRF power, reaching 2.4×10^{19} at/s. As $|V_{RF}| \propto P_{RF}{}^{1/2}$ and the curve $Y_{eff}(V_{DC})$ is locally concave in the yellow region, S_W grows fast at low P_{RF}. S_W over all outer ports amounts to 1.8×10^{20} at/s for 20 MW coupled. This however represents a ~ 9 % increase compared to S_W due to thermal sheaths only. For comparison, F_{max}-1=+20 %. This increment neither takes into account other objects than mid-plane ports, nor ICRF-independent physical processes (charge exchange, ELMs…) as possible contributors to the core W contamination. The "low 2010" profile with propagative Slow Wave yield qualitatively similar relative variations as the "high 2010" profile with evanescent Slow Wave over the P_{RF} scan, with absolute numbers ~ 2000 times below those with the "high 2010" profile.

Fig. 6 questions which tests can be made during the SRO. Present-day experiments are quite optimistic in the ability to detect the ICRF-specific PWI on the antenna port, even at modest ICRF power, by implementing specific local measurements. For example, reference [33] reported an ICRF-related tripling of the W I line brightness at λ =400.8 nm using visible spectroscopy, when $n_e \sim 10^{18}$ m^{-3} on the limiters. Dedicated infrared thermography of the WEST antenna limiters proved capable of measuring ICRF-related heat fluxes in the range of 1 MW/m^2 [4]. Detecting a 20 % increase in the W contamination of the plasma core appears more challenging. In WEST L-mode plasmas, the radiated power fraction only weakly depends on the heating method [33].

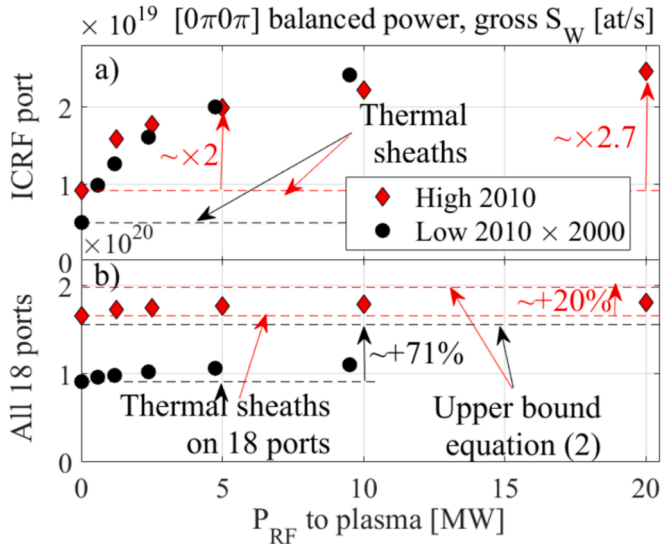

Fig. 6. Variation of estimated gross W production S_W a) on the ICRF port and b) over the 18 ports, *versus* ICRF power, for two density profiles in Fig. 2.

3.4. Tailoring the PWI and RF wave coupling by local gas puffing

Reference [8] tested numerically several techniques to balance good ICRF wave coupling and reasonnable PWI. The appropriate strategy depends on the plasma scenario: for the "low density" cases, power coupling is the main challenge, while degradading (slightly) the PWI remains tolerable. Inspired by successful tests on various machines with various antennas [24,34–36] backed by theoretical arguments [37], some options exploit the flexible RF feeding schemes of the ITER ICRF antenna [3], by changing the phasing and power ratios between the columns of straps [7]. For a given RF feeding scheme, an alternative way to improve the wave coupling is to act on the density distribution in front of the antenna structure, so that the R-cutoff layer for the Fast Wave moves radially towards the antenna. To this end, local gas puffing close to the active antennas was successfully tested experimentally [38].

Fig. 7 compares the simulation results with "low 2010" (baseline or shifted radially by 5 cm) and "gas puff" conditions. We quantify the coupling capability as the ICRF power coupled over the squared maximal ICRF voltage in the antenna structure, from TOPICA [15]. With the "Low 2010" profile, 9.5 MW can be coupled with the stand-off voltage of 45 kV, while the shifted profile allows coupling 20 MW with 42.1 kV and "gas puff" with 39 kV. We quantify S_W with ICRF at the maximal ICRF power that can be coupled. Both with "shifted" or "gas puff" profiles, the local density on the ICRF port increases by a factor 4.4 compared to "low 2010". The temperature also evolves. The counterpart of a better coupling is therefore a 11-fold increase of the local S_W compared "Low 2010" profile. This "local" PWI is in the same ballpark for "gas puff" and "radially shifted" profiles. While rigid radial shifts of the magnetic equilibrium are easy to implement, they affect indifferently all the out-board mid-plane ports, including the W erosion from thermal sheaths on 17 "passive" ports. However, to improve ICRF coupling, it is necessary to tailor the density profiles only in front of the ICRF antenna. When 4.55×10^{22} e$^-$/s are injected, equally split between ports 13 (ICRF) and 15, numerical simulations indicate that the "gas puff" profile in Fig. 3 replaces the "low 2010" profile only in front of the ICRF port and one adjacent port [31,32]. This results in reduced S_W over 18 ports, compared to a rigid plasma shift. In all cases, the absolute numbers remain 100 times below those with the "high 2010" profile in Figs. 3, 6.

4. Conclusions and outlook

In view of the proposed re-baselining of ITER [1], this contribution

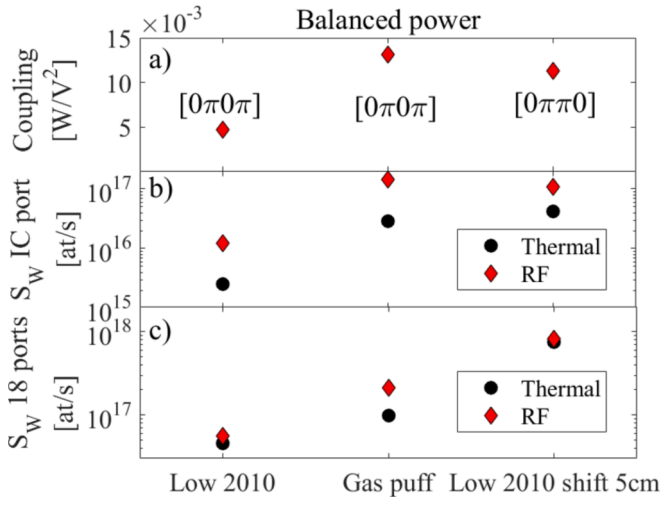

Fig. 7. Comparison of a) RF coupling capability, b) gross W erosion on ICRF port and c) over 18 ports, with or without RF power, using "Low 2010" (baseline or shifted by 5 cm) and "gas puff" density profiles.

re-assessed numerically the Plasma-Wall Interaction (PWI) associated with RF-sheath rectification close to the ITER ICRF antenna [3], focusing on the ICRF-specific gross impurity erosion from full-tungsten (W) antenna port sides. Simulations shed light onto the four points outlined in the introduction.

1) The ITER far SOL plasma conditions remain largely uncertain [1]. Higher densities yield more intense PWI, with or without ICRF waves. When Slow Waves are propagative in front of the antenna, the main ICRF power loss channel in the SOL might become the LH resonance [23], although present experiments did not so far evidence any major effect related to this resonance [7].
2) In high-density conditions, larger margins exist for coupling the ICRF power. We documented operational trade-offs between these two constraints [8], some of which were already tested experimentally [4]. We illustrated the merit of local gas puffing: it increases the density mainly where power coupling needs it, without degrading the PWI on sixteen "passive" ITER ports, consistent with experimental results on present devices [38]. Local gas puffing might also reduce the ICRF power losses at the LH resonance [23].
3) While useful for divertor detachment, neon ions cause intense W sputtering with the simulated plasma, already at low sheath voltages. Although the RF-sheath rectification amplifies the local gross erosion at the antenna port by up to a factor 5, this increment (F-1) represents at worse 22 % of the W source expected from thermal sheaths over the eighteen out-board mid-plane ports in ITER, and 9 % for profile "high 2010" of [18]. When neon dominates the sputtering, F weakly depends on its concentration. F would be lower if one considers the whole outer wall instead of only the outer ports. We proposed an upper bound F_{max} for this enhancement factor. Independent of our main assumptions, F_{max} depends mainly on the local temperatures at the outer wall and on the plasma composition, *via* the variations the effective sputtering yield with the accelerating voltage (Fig. 4).
4) This moderate global increase questions the ability to detect any ICRF-specific W contamination of the plasma core, even at the planned maximal ICRF power. Present-day experiments however suggest that one could monitor the local PWI in the ICRF port on the high-density scenarios, using specific local diagnostics (*e.g.* visible spectroscopy [4,7] or infrared thermography).

Despite the simple SSWICH-SW modelling approach and many assumptions, as conservative as possible, the qualitative gross W erosion trends evidenced above are likely robust: they rely on basic PWI properties *via* equations (1)-(2) and Fig. 4. References [6,8,19] analyzed the sensitivity of the SSWICH-SW results to some of our assumptions. A different approach reached similar qualitative conclusions [7]. RF-sheath modelling tools evolve rapidly and should soon provide higher fidelity. More accurate PWI estimates require more refined assessment of the background plasma at the ITER wall [26]. In preparation of the machine commissioning, it would also be useful to simulate SRO scenarios in complement of the reported DT plasmas.

CRediT authorship contribution statement

L. Colas: Writing – review & editing, Writing – original draft, Methodology, Investigation, Formal analysis. **W. Helou:** Validation, Supervision, Resources, Project administration, Funding acquisition, Data curation. **G. Urbanczyk:** Visualization, Software, Resources. **V. Bobkov:** Validation. **F. Calarco:** Validation, Supervision. **N. Fedorczak:** Validation, Supervision. **D. Milanesio:** Software, Resources. **J. Hillairet:** Validation, Software.

Declaration of competing interest

The authors declare that they have no known competing financial interests or personal relationships that could have appeared to influence the work reported in this paper.

Acknowledgements

This work has been conducted under contract IO/23/CT/4300002873. The views and opinions expressed herein do not necessarily reflect those of the ITER Organization.

Data availability

Data will be made available on request.

References

[1] R. Pitts et al., this conference, P1-117.
[2] S. Di Genova, G. Ciraolo, A. Gallo, J. Romazanov, N. Fedorczak, H. Bufferand, P. Tamain, N. Rivals, Y. Marandet, S. Brezinsek, E. Serre, the WEST team 1, Nucl. Mater. Energy 34 (2023) 101340, https://doi.org/10.1016/j.nme.2022.101340.
[3] W. Helou et al., "the ITER ICRF system: latest technological developments, coupling studies and compatibility with high-Z wall", 29th IAEA Fusion Energy Conference (FEC 2023), Oct 16 – 21, 2023, London, UK. https://conferences.iaea.org/event/316/contributions/29371/attachments/15525/25419/v1.0_IAEA-FEC-2023_W-Helou_Synopsis.pdf.
[4] L. Colas, G. Urbanczyk, M. Goniche, J. Hillairet, J.-M. Bernard, C. Bourdelle, N. Fedorczak, C. Guillemaut, W. Helou, V. Bobkov, R. Ochoukov, Ph. Jacquet, E. Lerche, X. Zhang, C. Qin, C.C. Klepper, C. Lau, B. Van Compernolle, S. J. Wukitch, Y. Lin, M. Ono, J.E.T. Contributors, the ASDEX Upgrade Team, the EAST Team, the WEST Team and ITPA IOS, Nucl. Fusion 62 (2022) 016014, https://doi.org/10.1088/1741-4326/ac35f9.
[5] D6 – Sheath Modeling (ITER_D_9RG38U v1.2), https://user.iter.org/default.aspx?uid=9RG38U&version=v1.2.
[6] L. Colas et al. "Self-Consistent Modeling of Radio-Frequency Sheaths: Comparison with Tore Supra Measurements and Predictability for Future Machines", proc. IAEA Fusion Energy Conference Saint Petersburg (2014) TH/P6-9 http://naweb.iaea.org/napc/physics/FEC/FEC2014/fec2014-preprints/457_THP69.pdf.
[7] V. Bobkov, R. Bilato, F. Calarco, L. Colas, R. Dux, G. Grenfell, W. Helou, D. Milanesio, R. Ochoukov, F. Paulus, Th. Pütterich, G. Urbanczyk, M. Usoltseva, the ASDEX Upgrade Team, Nucl. Mater. Energy 41 (2024) 101742, https://doi.org/10.1016/j.nme.2024.101742.
[8] L. Colas et al., analysis report of the deliverable DL1 of the SSA-104 "RF Sheath Modelling for the ITER ICRF antennas using the SSWICH code", https://user.iter.org/?uid=9ZJKYY.
[9] L. Colas, J. Jacquot, S. Heuraux, E. Faudot, K. Crombé, V. Kyrytsya, J. Hillairet, M. Goniche, Phys. Plasmas 19 (2012) 092505, https://doi.org/10.1063/1.4750046.
[10] J. Jacquot, D. Milanesio, L. Colas, Y. Corre, M. Goniche, J. Gunn, S. Heuraux, M. Kubič, Phys. Plasmas 21 (2014) 061509, https://doi.org/10.1063/1.4884778.
[11] J. R. Myra *Journal of Plasma Physics* , Volume **87** , Issue 5 , October 2021 , 905870504 doi:10.1017/S0022377821000878.
[12] L.F. Lu, L. Colas, L. Cao, G. Urbanczyy, B. Lu, Y.Q. Shen, X.J. Zhang, Nucl. Fusion 64 (2024) 126013, https://doi.org/10.1088/1741-4326/ad7c65.
[13] W. Tierens, A. Kumar, C. Klepper, J. Lore, J.R. Myra, J. Hillairet, G. Urbanczyk, W. Helou, L. Colas, A. Grosjean, J. Gunn and the WEST Team, Nucl. Fusion 64 (2024) 126039, https://doi.org/10.1088/1741-4326/ad80a9.
[14] S. Shiraiwa, N. Bertelli, W. Tierens, R. Bilato, J. Hillairet, J. Myra, H. Kohno, M. Poulos, M. Ono, Nucl. Fusion 63 (2023) 026024, https://doi.org/10.1088/1741-4326/aca6f9.
[15] D. Milanesio, W. Helou, V. Polli, F. Durodié, P. Lamalle, V. Maquet, A. Messiaen, W. Tierens, W. Zhang, 6, Nucl. Fusion 63 (2023) 046010, https://doi.org/10.1088/1741-4326/acb785.
[16] L. Lu, K. Crombé, D. Van Eester, L. Colas, J. Jacquot, S. Heuraux, Plasma Phys. Control. Fusion 58 (2016) 055001, https://doi.org/10.1088/0741-3335/58/5/055001.
[17] V. Rozhansky *Reviews of Plasma Physics* **24** Springer 2008 pp. 1-52 https://doi.org/10.1007/978-3-540-74576-1.
[18] Technical Input for SSA-104, https://user.iter.org/default.aspx?uid=9GQSFQ.
[19] W. Tierens, J. Jacquot, V. Bobkov, J.M. Noterdaeme, L. Colas and The ASDEX Upgrade Team, *Nucl. Fusion* **57** (2017) 116034 DOI 10.1088/1741-4326/aa7f9e.
[20] G. Urbanczyk et al., this conference, P2-072.
[21] A. Křivská, V. Bobkov, L. Colas, P. Dumortier, F. Durodié, P. Jacquet, C.C. Klepper, D. Milanesio, G. Urbanczyk, JET contributors, Nucl. Mater. Energy 19 (2019) 324–329, https://doi.org/10.1016/j.nme.2019.03.009.
[22] M. Usoltceva, R. Ochoukov, W. Tierens, A. Kostic, K. Crombé, S. Heuraux, J. M. Noterdaeme, *Plasma. Phys.* Control. Fusion 61 (2019) 115011, https://doi.org/10.1088/1361-6587/ab476d.
[23] V. Maquet, A. Druart, A. Messiaen, J. Plasma Phys. 87 (2021) 905870617, https://doi.org/10.1017/S0022377821001161.
[24] R. Diab, G. Decristoforo, S. Ahmed, S.G. Baek, Y. Lin, E. Marmar, J.L. Terry, S. J. Wukitch, Nucl. Fusion 64 (2024), https://doi.org/10.1088/1741-4326/ad26a9.
[25] L. Colas, V. Bobkov, D. Carralero, M. Kočan, H.W. Müller, P. Manz, M. Kubič, J. P. Gunn, A. Herrmann, V. Rohde, ASDEX-Upgrade Team *AIP Conf. Proc.* 1580 (2014) 259–262, https://doi.org/10.1063/1.4864537.

[26] S. Sureshkumar, N. Rivals, P. Tamain, X. Bonnin, R. Pitts, Y. Marandet, G. Ciraolo, H. Bufferand, G. Falchetto, N. Fedorczak, V. Quadri, M. Raghunathan, F. Schwander, E. Serre, R. Düll, N. Varadarajan, Nucl. Mater. Energy 41 (2024) 101780, https://doi.org/10.1016/j.nme.2024.101780.
[27] R. Behrisch, W. Eckstein, « Sputtering by Particle Bombardment: Experiments and Computer Calculations from Threshold to MeV Energies », *Topics in Applied Physics* vol. **110**, Springer Berlin (2007) https://doi.org/10.1007/978-3-540-44502-9.
[28] E. Kawamura, V. Vahedi, M. A. Lieberman and C. K. Birdsall*Plasma Sources Sci. Technol.* **8** (1999) R45–R64 DOI 10.1088/0963-0252/8/3/202.
[29] M. Elias, D. Curreli, T.G. Jenkins, J.R. Myra, J. Wright, Phys. Plasmas 26 (2019) 092508, https://doi.org/10.1063/1.5109256.
[30] M. Elias, D. Curreli, J.R. Myra, Phys. Plasmas 28 (2021) 052106, https://doi.org/10.1063/5.0045962.
[31] W. Zhang, R. Bilato, T. Lunt, A. Messiaen, R.A. Pitts, S. Lisgo, X. Bonnin, V. Bobkov, D. Coster, Y. Feng, P. Jacquet, J.M. Noterdaeme, Nucl. Mater. Energy 19 (2019) 364–371, https://doi.org/10.1016/j.nme.2018.12.025.
[32] W. Zhang, A. Messiaen, W. Helou, V. Bobkov, P. Lamalle, R.A. Pitts, W. Tierens, Nucl. Fusion 63 (2023) 036008, https://doi.org/10.1088/1741-4326/acb4ad.
[33] L. Colas et al. « Tungsten gross erosion and plasma impurity contamination in WEST phase I : A statistical comparison of LH and ICRF-heated L-mode plasmas », proceedings IAEA-FEC conference London 2023, IAEA-CN-316/2045 https://conferences.iaea.org/event/316/contributions/28181/attachments/14603/23890/Colas-EX-H.pdf.
[34] V. Bobkov, D. Aguiam, R. Bilato, S. Brezinsek, L. Colas, A. Czarnecka, P. Dumortier, R. Dux, H. Faugel, H. Fünfgelder, Ph. Jacquet, A. Kallenbach, A. Krivska, C. C. Klepper, E. Lerche, Y. Lin, D. Milanesio, R. Maggiora, I. Monakhov, R. Neu, W. Zhang, Nucl. Mater. Energy 18 (2019) 131–140, https://doi.org/10.1016/j.nme.2018.11.017.
[35] Y. Lin, J.C. Wright, S.J. Wukitch, J. Plasma Phys. 86 (2020) 865860506, https://doi.org/10.1017/S0022377820001269.
[36] A. Chomiczewska, W. Gromelski, I. Ivanova-Stanik, E. Kowalska-Strzęciwilk, N. Wendler, P. Jacquet, E. Lerche, V. Bobkov, L. Colas, P. Dumortier, D. Douai, D. Van Eester, J. Mailloux, S. Menmuir, J. Karhunen, D. Milanesio, I. Monakhov, R. Otin, E. Pawelec, B., Thomas and JET contributors, Nucl. Fusion 64 (2024) 076058, https://doi.org/10.1088/1741-4326/ad536.
[37] L. Colas, L.-F. Lu, A. Křivská, J. Jacquot, J. Hillairet, W. Helou, M. Goniche, S. Heuraux, E. Faudot, Plasma Phys. Control. Fusion 59 (2017) 025014, https://doi.org/10.1088/1361-6587/59/2/025014.
[38] P. Jacquet, M. Goniche, V. Bobkov, E. Lerche, R.I. Pinsker, R.A. Pitts, W. Zhang, L. Colas, J. Hosea, S. Moriyama, S.-J. Wang, S. Wukitch, X. Zhang, R. Bilato, H. Bufferand, L. Guimarais, H. Faugel, G.R. Hanson, M. Kocan, I. Monakhov, J.-M. Noterdaeme, V. Petrzilka, A. Shaw, I. Stepanov, A.C.C. Sips, D. Van Eester, T. Wauters, the JET contributors and the ASDEX Upgrade team, the DIII-D team and the ITPA 'Integrated Operation Scenarios' members and experts, Nucl. Fusion 56 (2016) 046001, https://doi.org/10.1088/0029-5515/56/4/046001.